BBA - Molecular Cell Research 1871 (2024) 119649

Contents lists available at ScienceDirect

BBA - Molecular Cell Research

journal homepage: www.elsevier.com/locate/bbamcr

Research Paper

Blockade of angiotensin II modulates insulin-like growth factor 1-mediated skeletal muscle homeostasis in experimental steatohepatitis

Misako Tanaka, Kosuke Kaji *, Norihisa Nishimura, Shohei Asada, Aritoshi Koizumi, Takuya Matsuda, Nobuyuki Yorioka, Yuki Tsuji, Yukihisa Fujinaga, Shinya Sato, Tadashi Namisaki, Takemi Akahane, Hitoshi Yoshiji

Department of Gastroenterology, Nara Medical University, Kashihara, Nara 634-8521, Japan

ARTICLE INFO

Keywords:
Sarcopenia
Nonalcoholic steatohepatitis
Angiotensin II
Insulin-like growth factor 1

ABSTRACT

Sarcopenia is associated with mortality in patients with nonalcoholic steatohepatitis (NASH). Angiotensin II receptor blocker (ARB) has been suggested to prevent sarcopenia, but reports on its effect on NASH-derived skeletal muscle atrophy in conjunction with insulin-like growth factor 1 (IGF-1)-mediated muscle homeostasis are few. Our aim was to examine the combined effect of the ARB losartan and IGF-1 replacement on skeletal muscle atrophy in a methionine–choline deficient (MCD) diet-fed murine steatohepatitis model. The MCD-fed mice developed steatohepatitis and skeletal muscle atrophy, as indicated by the reduction of psoas muscle mass and attenuation of forelimb and hindlimb grip strength. Significantly suppressed steatohepatitis and skeletal muscle atrophy was observed after single treatment with ARB or IGF-1, and these effects were augmented after combination treatment. Treatment with ARB and IGF-1 effectively inhibited ubiquitin proteasome-mediated protein degradation by reducing forkhead box protein O1 (FOXO1) and FOXO3a transcriptional activity in the skeletal muscle. Combined ARB and IGF-1 decreased the intramuscular expression of proinflammatory cytokines (i.e., TNFα, IL6, and IL1β) and increased the Trolox equivalent antioxidant capacity and antioxidant enzymes (CAT, GPX1, SOD2, and CYTB). This antioxidant effect was based on downregulation of NADPH oxidase (NOX) 2, normalization of mitochondrial biogenesis and dynamics. Moreover, ARB increased the hepatic and plasma IGF-1 levels and improved steatohepatitis, leading to enhanced skeletal muscle protein synthesis mediated by IGF-1/ AKT/ mechanistic target of rapamycin signaling. Collectively, combined ARB and IGF-1 replacement could be a promising new therapeutic target for NASH-derived skeletal muscle wasting.

1. Introduction

Nonalcoholic fatty liver disease (NAFLD), which is recently termed metabolic dysfunction-associated steatotic liver disease, is considered as the most prevalent liver disease globally [1,2]. NAFLD includes progressive conditions, ranging from simple steatosis to nonalcoholic steatohepatitis (NASH), which is characterized by steatosis and fibrosis [2]. In NASH, fibrosis is the most crucial histologic feature that determines long-term prognosis. Therefore, improvement of hepatic fibrosis is an important surrogate endpoint in patients with NAFLD [3].

Currently, the close interaction between NASH and sarcopenia has gained attention. Sarcopenia is characterized by gradual loss of skeletal

Abbreviations: ALT, alanine aminotransferase; ARB, angiotensin II receptor blocker; AST, aspartate amino transferase; ATII, Angiotensin II; CAT, catalase; COX7A1, cytochrome C oxidase subunit 7A1; CT, computed tomography; Cytb, cytochrome *b*; DPPH, Diphenyl-1-picrylhydrazyl; DRP1, dynamin-related protein 1; FOXO1, forkhead box protein O1; FOXO3a, forkhead box protein O3a; GAPDH, glyceraldehyde 3-phosphate dehydrogenase; GDF15, growth differentiation factor 15; GPX1, Glutathione peroxidase 1; H&E, Hematoxylin/eosin; IGF-1, insulin-like growth factor 1; IL1β, Interleukin-1β; IL6, Interleukin-6; LC3, microtubule-associated protein 1A/1B-light chain 3; MCD, methionine–choline deficient; MDA, malondialdehyde; mtDNA, mitochondrial DNA; MFN2, mitofusin-2; MSTN, myostatin; mTOR, mechanistic target of rapamycin; mtTFA, mitochondrial transcription factor A; MuRF1, muscle ring-finger protein-1; MyoG, myogenin; NAFLD, nonalcoholic fatty liver disease; NASH, nonalcoholic steatohepatitis; NOX1, NADPH oxidase 1; NOX2, NADPH oxidase 2; NOX3, NADPH oxidase 3; PGC-1α, peroxisome proliferator-activated receptor γ coactivator 1α; PINK1, PTEN induced kinase 1; PI3K, phosphoinositide 3-kinase; PMI, psoas muscle mass index; ROS, reactive oxygen species; SOD2, Superoxide dismutase 2; TFEB, transcription factor EB; TNFα, Tumor Necrosis Factor; 4E-BP1, 4E-binding protein 1.

* Corresponding author at: Department of Gastroenterology, Nara Medical University, 840 Shijo-cho, Kashihara, Nara 634-8521, Japan.
E-mail address: kajik@naramed-u.ac.jp (K. Kaji).

https://doi.org/10.1016/j.bbamcr.2023.119649
Received 30 August 2023; Received in revised form 29 November 2023; Accepted 1 December 2023
Available online 12 December 2023

muscle mass and strength and is induced not only by aging but also by malnutrition and various diseases, including NASH [4]. The prevalence of sarcopenia gradually increases as NAFLD progresses [5]. Moreover, sarcopenia was reported to be a risk factor for the histological progression of NASH to cirrhosis, independent of obesity and insulin resistance [5–7]. Accordingly, improvement of sarcopenia is expected to be beneficial for the prognosis of patients with NASH. Currently, the treatments for sarcopenia include physical exercise and nutritional replacement, such as branched chain amino acid supplementation; however, the therapeutic effects are limited [8–10]. Therefore, further studies are warranted to identify novel treatment strategies for NASH-based sarcopenia.

Insulin-like growth factor 1 (IGF-1) is known to be a key hypertrophic factor that exhibits both anabolic and catabolic properties in skeletal muscle homeostasis [11]. It is predominantly produced in the liver and plays a pivotal role in skeletal muscle protein synthesis through the phosphoinositide 3-kinase (PI3K)/AKT/mechanistic target of rapamycin (mTOR) pathway [11]. Moreover, IGF-1 inhibits skeletal muscle protein degradation and augments skeletal muscle regeneration through activation of skeletal muscle stem/ satellite cells [11]. Accordingly, low IGF-1 concentration has been considered to be involved in skeletal muscle atrophy and may be a key component in the development of sarcopenia [12]. Meanwhile, patients with cirrhosis were found to have low plasma IGF-1 levels, which reflect hepatocellular dysfunction [13]. In particular, several clinical trials have suggested that a decrease in IGF-1 level may contribute to the progression of hepatic steatosis, inflammation, and fibrosis in NASH [14]. Moreover, experimental diet-induced NASH mice models were shown to have significant sarcopenia, with decreased hepatic IGF-1 expression and low IGF-1 serum level [15]. Therefore, IGF-1 is a potential therapeutic target for the skeletal muscle mass wasting and hepatic injury in NASH. However, the clinical use of IGF-1 replacement had been limited to endocrine diseases and seemed to only partially improve skeletal muscle mass or function when given alone [16]. Therefore, we postulated that combining IGF-1 with another agent would add therapeutic benefits for NASH-derived sarcopenia.

Angiotensin II (ATII) is a known key player during NASH progression by altering hepatic lipid metabolism, exacerbating insulin resistance, inducing reactive oxygen species (ROS) generation, modulating the proinflammatory response, and developing fibrosis [17]. Numerous clinical and basic studies have demonstrated that ATII receptor blockers (ARBs) could attenuate liver injury and fibrosis in NASH [18,19]. In addition, the presence of ATII receptors in skeletal muscle was shown to hinder skeletal muscle growth [18]. ATII inhibits muscle protein synthesis and regeneration by disrupting the binding of IGF-1 and insulin to their receptors, which results in decreased mTOR activity [20]. In this context, animal studies have indicated the suppressive effects of ARBs on skeletal muscle dysfunction and atrophy [18]. Moreover, clinical studies demonstrated that the use of ARBs could mitigate skeletal muscle wasting in patients with cardiovascular diseases and those on hemodialysis [21]. However, the capacity of ARBs to modulate the myotrophic activity of IGF-1 in NASH-derived skeletal muscle atrophy remains unclear. Therefore, the present study aimed to investigate the combined effect of ARB and IGF-1 replacement on skeletal muscle atrophy in a methionine–choline deficient (MCD) diet-fed mice model of steatohepatitis.

2. Material and methods

2.1. Animals and treatment

A total of 25 male C57BL/6NCrslc mice (10-week-old) were purchased from Japan SLC (Tokyo, Japan) and divided into five groups. Mice were housed for six weeks with treatment as below. For the groups that needed continuous administration of vehicle or IGF-1, all mice were implanted subcutaneously with osmotic pumps (Alzet osmotic pump model 2006, DURECT Co., Palo Alto, CA, USA). The NC + Veh group was fed with normal chow diet and received oral administration of lactose and subcutaneous administration of saline as the vehicle. The MCD + Veh group was fed with an MCD diet (Research Diets Inc., New Brunswick, NJ, USA) and received the vehicle through oral and subcutaneous routes. The MCD + ARB group was fed with an MCD diet and received the ARB losartan (LKT Labs, Inc., St Paul MN, USA) through the oral route at 7.5 mg/kg/day and the vehicle through the subcutaneous route [22]. The MCD + IGF-1 group was fed with an MCD diet and received the vehicle orally and the recombinant human IGF-1 at 2.5 μg/body/h (LS-G27099, LSBio, Shirley, MA, USA) [23] through the subcutaneous route using osmotic pumps. The MCD + Both group was fed with an MCD diet and received oral losartan and subcutaneous IGF-1. All mice were euthanized at the end of experimental period under a pentobarbital sodium anesthesia. Plasma, liver and gastrocnemius muscle samples were collected for each experiment. Plasma levels of aspartate amino transferase (AST), alanine aminotransferase (ALT), and albumin were measured as described [24]. The present study was approved by the Animal Ethics Committee of Nara Medical University (approval no.13154, 13,226), and all protocols were performed in accordance with the National Institutes of Health Guidelines for the Care and Use of Laboratory Animals.

2.2. Determination of psoas muscle mass and measurement of grip strength

The cross-sectional area of psoas muscle mass was measured as the level of the L3 pedicle on a single computed tomography (CT) slice using CosmoScan FX (Rigaku Corporation, Tokyo, Japan). The psoas muscle mass index (PMI) was determined as a L3 cross sectional area/ height^2 using Slice-O-Matic (Tomovision, Montreal, Canada) [25]. Forelimb and hindlimb grip strength was simultaneously measured using a grip strength meter (MK-380Si) (Muromachi Machinery, Kyoto, Japan) [26]. The peak tension was recorded at the time the mouse released the grip on the bar. Measurements were repeated three times, and the mean of three measurements was recorded.

2.3. Histological and immunofluorescent analyses

Liver and gastrocnemius muscle sections from all mouse were routinely fixed in 10 % formalin and embedded in paraffin. Hematoxylin/eosin (H&E) and Sirius-Red staining was then carried out according to the standard procedures. A pathologist blind to the assigned experimental group assessed liver histology and scored samples according to the degree of steatosis according to NAFLD activity score system [27]. Forkhead box protein (FOX)O1 (#2880) and FOXO3a (#12829) antibodies from Cell Signaling Technology (Danvers, MA, USA) were used as the primary antibodies for immunofluorescence analysis of the gastrocnemius muscle specimens. The immunofluorescence detection of the primary antibodies was performed using IgG (H + L) Alexa Fluor-conjugated secondary antibodies (Thermo Fisher Scientific Inc., Waltham, MA, USA). Cell apoptosis of hepatocytes was determined by TUNEL assay using the in situ Apoptosis Detection Kit (Takara Bio Inc., Kusatsu, Japan) on the liver sections according to the manufacturer's instruction. The sections were mounted on Vectashield mounting medium with 4′,6-diamidino-2-phenylindole Fluoromount-G mounting medium for fluorescent nucleic acid staining (Vector Laboratories, Inc., Newark, CA, USA). Semi-quantitative analysis was performed for five fields per section in high-power fields at x400 magnification using ImageJ software version 64 (National Institutes of Health, Bethesda, MD, USA).

2.4. Measurement of plasma and hepatic IGF1 levels

The plasma IGF1 concentrations were measured using the Mouse/Rat IGF1/IGF1 Quantikine ELISA kit and Human IGF-1 Quantikine ELISA kit (R&D systems, Minneapolis, MN, USA) according to the

manufacturer's protocol. The hepatic IGF1 concentration in 50 mg of liver tissue was measured using the same ELISA kit.

2.5. FOXO1 and FOXO3a transcriptional activity

Nuclear proteins were extracted from the gastrocnemius muscle tissues using an EpiQuik Nuclear Extraction Kit I (EpiGentek, Farmingdale, NY, USA). The protein concentration was measured by a protein assay (Bio-Rad, Hercules, CA, USA), and nuclear proteins were normalized to 20 μg. FOXO1 and FOXO3a transcriptional activities were determined using FOXO1 Transcription Factor Assay Kit (Abcam, Cambridge, UK) and Mouse FO/FOXO3A ELISA Kit (LSBio). All assays were performed as described in the manufacturer's instructions.

2.6. Trolox equivalent antioxidant capacity

The Trolox equivalent antioxidant capacity in 25 mg of gastrocnemius muscle tissue was measured to determine the total antioxidant capacity using 2,2-Diphenyl-1-picrylhydrazyl (DPPH) Antioxidant Assay Kit (DOJINDO Laboratories, Kumamoto, Japan), according to the manufacturer's protocol [28]. Briefly, 20 μL of samples were added to each well of a microtiter plate, followed by 80-μL assay buffer, 100-μL ethanol, and 100-μL DPPH working solution. Thereafter, the plate was incubated at 25 °C for 30 min in the dark. The optical density was measured at 517 nm using a microplate absorbance reader.

2.7. Hepatic and muscle levels of malondialdehyde

The amount of malondialdehyde (MDA) in mouse liver tissue (100 mg) or gastrocnemius muscle tissue (10 mg) was measured using MDA Assay Kit (DOJINDO Laboratories). All samples were processed and assayed according to the manufacturer's protocol.

2.8. RNA isolation and real-time quantitative polymerase chain reaction

RNA extraction was carried out using the RNeasy Fibrous Tissue Mini kit (Qiagen, Hilden, Germany) as per the manufacturer's instructions. cDNA synthesis was performed using the High-Capacity RNA-to-cDNA™ Kit (Thermo Fisher Scientific Inc.) and the RT-qPCR was carried out with the SYBR™-Green PCR Master Mix (Thermo Fisher Scientific, Inc.) as per the manufacturer's instructions. The fold change of gene expression was normalized with *Gapdh* and relative fold change was calculated using the $2^{-\Delta\Delta CT}$ method. All primer sequences used for RT-qPCR are listed in Supplementary Table 1.

2.9. Mitochondrial DNA copy number

Mitochondrial DNA (mtDNA) analysis was performed as previously described [29]. Total DNA was extracted from the gastrocnemius muscle tissue using a DNeasy Blood & Tissue Kit (Qiagen). Then, mtDNA copy number in total DNA was quantified by measuring expression levels of a mitochondrial-encoded gene (*Cox2*) by RT-qPCR. mtDNA copy number was normalized to the expression level of a nuclear-encoded gene (Cyclophilin A; *Ppia*). The primer sequences were 5′- CCATAGGGCACCAATGATACTG −3′ and 5′- AGTCGGCCTGGGATGGCATC -3′ for *Cox2* and 5′- ACACGCCATAATGGCACTGG −3′ and 5′- CAGTCTTGGCAGTGCAGAT −3′ for nuclear-encoded *Ppia*.

2.10. Western blotting

Protein was extracted with the use of RIPA lysis buffer (Sigma-Aldrich, St. Louis, MO, USA), plus Halt™ Protease and Phosphatase Inhibitor Cocktail (Thermo Fisher Scientific, Inc.) from the gastrocnemius muscle. The proteins were transferred to a nitrocellulose membrane. After sealing with 5 % skimmed milk, the membranes were successively incubated with diluted primary antibodies and HRP-conjugated secondary antibodies. The primary antibodies included myostatin (MSTN, #ab203076; 1:500), atrogin-1 (#ab74023; 1:1000), muscle ring-finger protein-1 (MuRF1, #ab172479; 1:1000), myogenin (MyoG, #ab124800; 1:200), MyoD1 (#ab203383; 1:200), peroxisome proliferator-activated receptor γ coactivator 1α (PGC-1α, #ab188102; 1:1000), mitochondrial transcription factor A (mtTFA, #ab131607; 1:2000), dynamin-related protein 1 (DRP1, #ab184247; 1:1000), and microtubule-associated protein 1A/1B-light chain 3 (LC3, # ab48394; 1:1000) from Abcam; total-AKT (#4691; 1:1000), phospho-AKT^{Ser473} (#4060; 1:1000), total-p70S6K (#9202; 1:1000), phosphor-p70S6K^{Thr389} (#9205; 1:1000), total-eukaryotic translation initiation factor 4E-binding protein 1 (4E-BP1, #9452; 1:1000), phospho-4E-BP1^{Ser65} (#9451; 1:1000), and glyceraldehyde 3-phosphate dehydrogenase (GAPDH, #2118, 1:1000) from Cell Signaling Technology; transcription factor EB (TFEB, #A303-673A; 1:2000) from Bethl Laboratories (Montgomery, TX, USA); cytochrome C oxidase subunit 7A1 (COX7A1, #11413–1-AP; 1:1000), mitofusin-2 (MFN2, #12186-1-AP; 1:2000), and PTEN induced kinase 1 (PINK1, # 23274-1-AP; 1:1000) from Proteintech (Rosemont, IL, USA). Finally, chemiluminescence was detected using a Clarity Western ECL Substrate (Bio-Rad) with Bright™ CL1500 Imaging System (Thermo Fisher Scientific, Inc.). Densitometric analysis was performed using ImageJ software version 64 (National Institute of Health).

2.11. Statistical analyses

Differences between each group was calculated by Mann–Whitney *U* test. All values are expressed as means ± SD. Statistical analyses were performed using Prism version 9.1.2 (GraphPad Software, La Jolla, CA, USA). A P value of <0.05 was statistically significant.

3. Results

3.1. ARB and IGF-1 inhibit steatohepatitis and reduce hepatic lipid peroxidation in MCD-fed mice

Fig. 1A shows the effects of the ARB losartan and IGF-1 on the body mass and hepatic phenotypes of the MCD diet-induced steatohepatitis mice model. Plasma human IGF-1 levels were increased in IGF-1-treated mice 1 week after the start of administration, indicating that IGF-1 was stably delivered during experimental period (Supplementary Fig. 1). Body weight was remarkably decreased after six weeks on an MCD diet, and single treatment with ARB or IGF-1 tended to suppress the MCD-induced body weight loss, although the difference was not significant (Fig. 1B). Meanwhile, combined treatment with ARB and IGF-1 significantly prevented body weight loss in the MCD diet-fed mice (Fig. 1B). The relative liver weight was increased by MCD diet feeding, and treatment with ARB and IGF-1 did not significantly suppress MCD-induced hepatomegaly (Fig. 1C). The MCD diet-fed mice had elevated levels of plasma AST and ALT and decreased albumin levels (Fig. 1D and E). Combined treatment with ARB and IGF-1 did not significantly affect the AST and ALT levels, but it inhibited the progression of hypoalbuminemia in the MCD diet-fed mice (Fig. 1F). Histological analysis demonstrated that single treatment with ARB or IGF-1 reduced hepatic steatosis, TUNEL^{+} hepatocyte apoptosis, and fibrosis in the MCD diet fed mice; notably, combined treatment augmented these effects (Fig. 1G–J). MCD diet feeding led to accumulation of the hepatic content of MDA, which is known as a biomarker of lipid peroxidation during steatohepatitis progression (Fig. 1K). Accumulation of intrahepatic MDA level was significantly decreased by treatment with ARB and IGF-1 (Fig. 1H). Moreover, we evaluated hepatic expression of growth differentiation factor 15 (GDF15), one of the metabolic effectors related to sarcopenia in NASH [30]. Notably, treatment with ARB and/or IGF-1 significantly reduced hepatic *Gdf15* expression in MCD diet-fed mice (Fig. 1L).

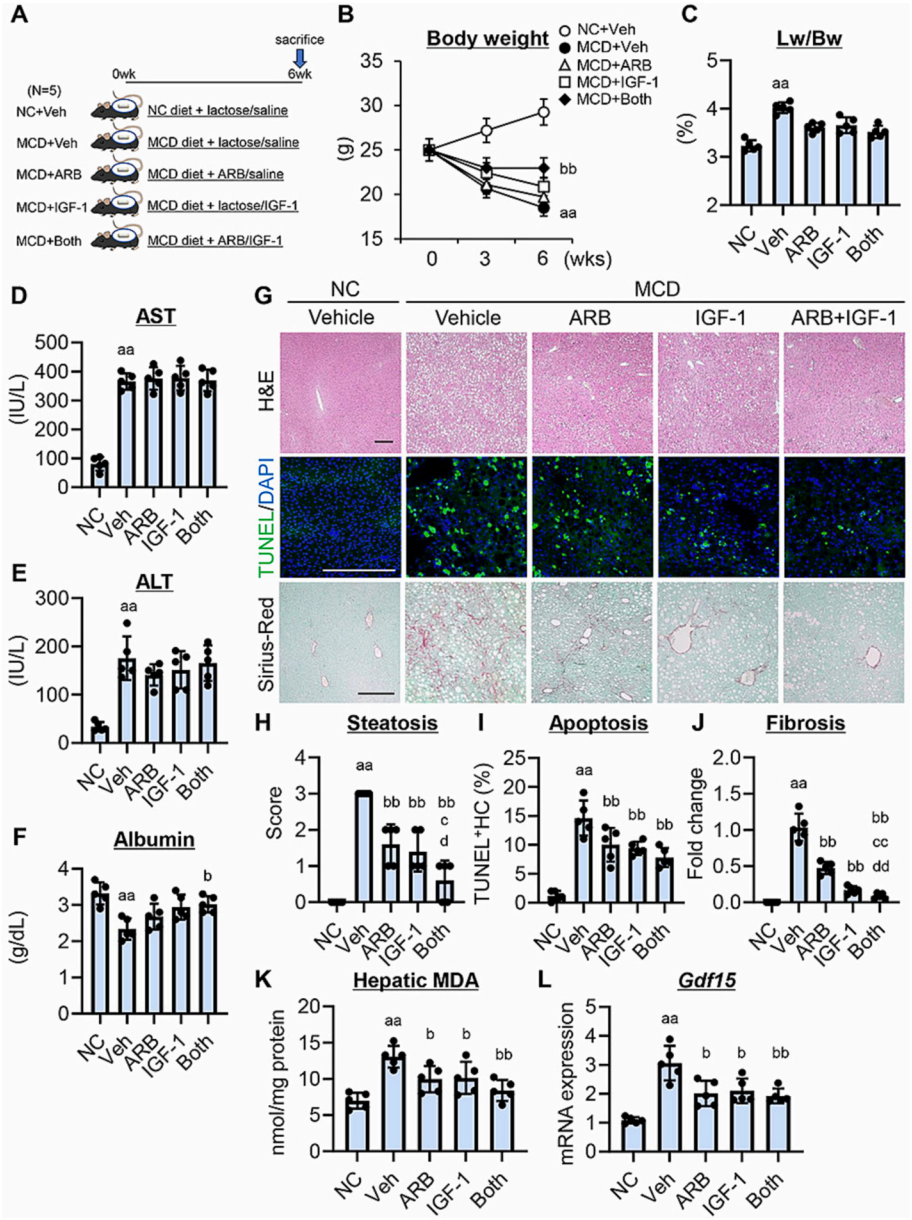

Fig. 1. Effect of ARB and IGF-1 on MCD-induced steatohepatitis. (A) Experimental design. (B) Changes in the body weights during the experimental period. (C) Liver/body (Lw/Bw) weight at the end of experiment. (D–F) Plasma levels of (D) aspartate transaminase (AST), (E) alanine aminotransferase (ALT), and (F) albumin at 6 weeks of treatment. (G) Representative microphotographs of liver sections stained with hematoxylin and eosin (H&E), TUNEL and Sirius-Red. Scale bar, 50 μm. (H) Pathological score of hepatic steatosis at a 400-fold magnification. (I) Quantification of TUNEL$^+$ hepatocytes. The ratio of TUNEL/DAPI positive hepatocytes per 50 DAPI positive hepatocytes in HPF was calculated. (J) Semi-quantification of Sirius-Red stained fibrotic areas. Quantitative values are indicated as fold changes to the values of MCD + Veh group. (K) Hepatic levels of malondialdehyde (MDA). (L) Relative mRNA expression levels of *Gdf15* in the liver tissue. Data are the mean ± SD ($n = 5$). NC, normal chow; MCD, methionine-choline deficient diet; Veh, vehicle; ARB, angiotensin receptor blocker; IGF-1, insulin-like growth factor 1; Both, combination with ARB and IGF-1. aa; $p < 0.01$ vs NC, b; $p < 0.05$ vs Veh, bb; $p < 0.01$vs Veh, c; $p < 0.05$ vs ARB, cc; $p < 0.01$ vs ARB, d; $p < 0.05$ vs IGF-1, dd; $p < 0.01$ vs IGF-1 using Mann–Whitney *U* test.

3.2. *Antisarcopenic effects of ARB and IGF-1 in the MCD diet-fed mice*

Based on the remarkable body weight loss, we presumed the development of skeletal muscle atrophy in the MCD diet-fed mice. Thus, the psoas muscle area was chronologically determined using a small animal CT and calculated the PMI as an imaging marker of sarcopenia (Fig. 2A and B). As shown in Fig. 2C, the PMI after six weeks was lower in the MCD diet-fed mice than in the NC diet-fed mice. It was noteworthy that single treatment with ARB or IGF-1 significantly attenuated the MCD-induced decrease in PMI, and this effect was augmented by combining both agents (Fig. 2C). In agreement with the attenuation of psoas muscle atrophy, the reduced weight of gastrocnemius muscle was ameliorated by treatment with ARB and IGF-1 in the MCD diet-fed mice (Fig. 2D).

For the muscle strength assessment, the MCD diet-fed mice showed significantly lower forelimb and hindlimb grip strength after six weeks, compared with that of the NC diet-fed mice (Fig. 2E and F). Treatment with ARB or IGF-1 alone suppressed the MCD-induced decrease in forelimb and hindlimb grip strength, and this effect was potentiated by combining both agents (Fig. 2E and F).

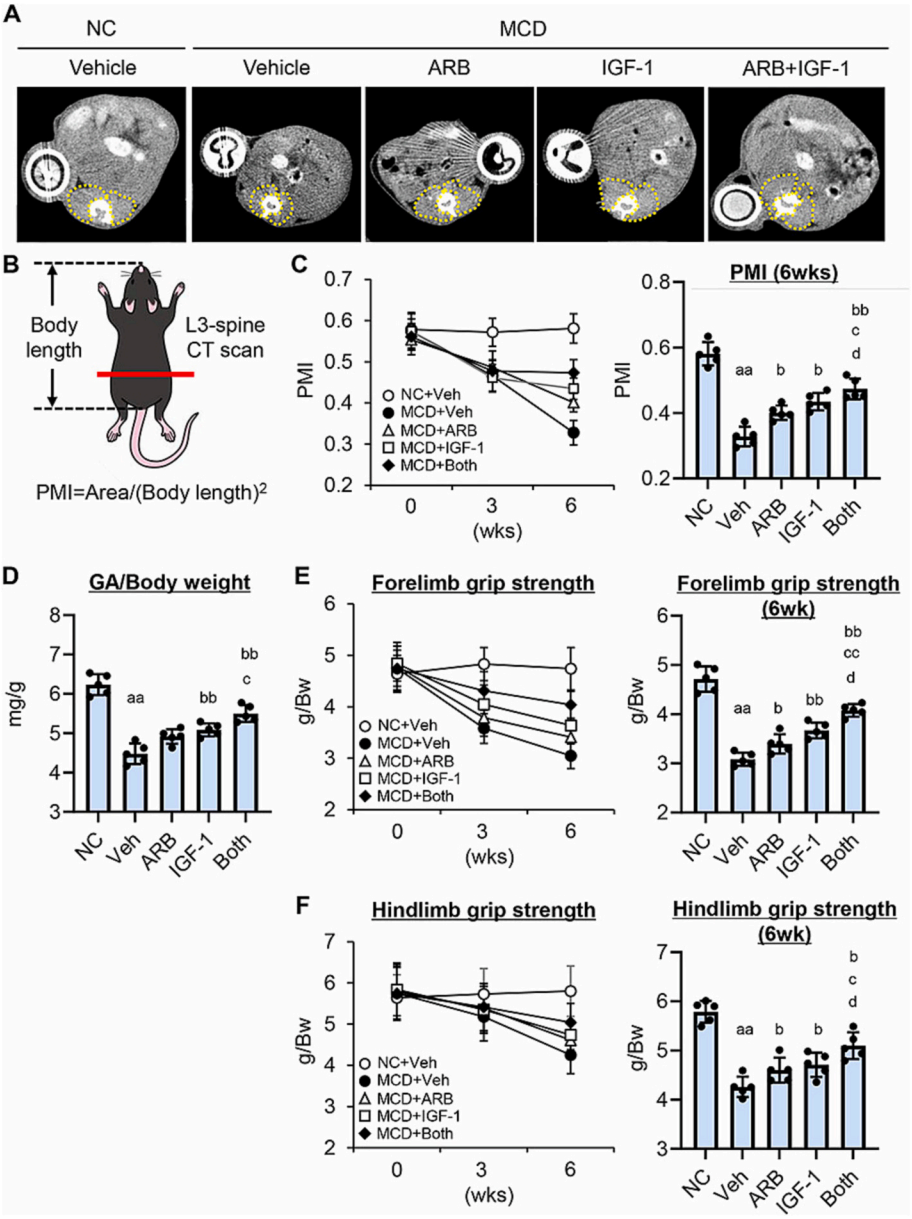

Fig. 2. Anti-sarcopenic effects of ARB and IGF-1 in MCD diet-fed mice. (A) Representative images on a single CT slice at the level of L3 pedicle. (B) Psoas muscle mass index (PMI; cross sectional area/height2) was assessed on a single CT slice at the level of L3 pedicle with image analysis system. (C) Chronological change (left panel) and the values at 6 weeks of treatment (right panel) of PMI. (D) Gastrocnemius muscle (GA)/body weight at 6 weeks of treatment. (E, F) Chronological changes (left panels) and the values at 6 weeks of treatment (right panels) of (E) forelimb grip strength and (F) hindlimb grip strength. Grip strength was indicated with the ratio to body weight. Data are the mean ± SD ($n = 5$). NC, normal chow; MCD, methionine-choline deficient diet; Veh, vehicle; ARB, angiotensin receptor blocker; IGF-1, insulin-like growth factor 1; Both, combination with ARB and IGF-1. aa; $p < 0.01$ vs NC, b; $p < 0.05$ vs Veh, bb; $p < 0.01$vs Veh, c; $p < 0.05$ vs ARB, cc; $p < 0.01$ vs ARB, d; $p < 0.05$ vs IGF-1 using Mann–Whitney *U* test.

3.3. ARB and IGF-1 suppress skeletal muscle protein degradation and enhance myogenesis in the MCD diet-fed mice

Next, we measured the diameter of the gastrocnemius muscle fibers to histologically determine skeletal muscle atrophy in mice at the end of the experiment. Fig. 3A showed an obvious atrophic change in the gastrocnemius muscle fibers in the MCD diet-fed mice. As shown in Fig. 3B, the Feret diameter of the fibers showed a regular distribution curve, with a peak of 40–45 μm in the NC diet-fed mice; this decreased in size, with a peak of 25–30 μm in the MCD diet-fed mice (Fig. 3B). Along with the recovery of the gastrocnemius weight, combined treatment with ARB and IGF-1 substantially normalized the distribution of the Feret diameter in the MCD diet-fed mice (Fig. 3B). Consistently, the average fibers diameter was smaller in the MCD diet-fed mice than in the NC diet-fed mice; this difference was diminished by treatment with ARB and IGF-1 (Fig. 3C).

We further assessed the expression of genes related with muscle protein degradation and myogenesis. E3 ubiquitin ligases including atrogin-1 and MuRF-1 are recognized to crucially regulate ubiquitin-mediated skeletal muscle protein degradation [31]. As shown in Fig. 3D, the mRNA expressions of *Fbxo32* (atrogin-1) and *Trim63* (MuRF-1) were increased in the gastrocnemius muscle tissues of the MCD diet-fed mice. Moreover, the intramuscular expression of MSTN (myostatin), which is a myokine that inhibits muscle cell growth, was significantly higher in the MCD diet-fed mice than in the NC diet-fed mice (Fig. 3E). These increased expressions were attenuated by single treatment with ARB or IGF-1, and this effect was potentiated by combined use (Fig. 3D and E). On the other hand, the gene expressions of the myogenic factors

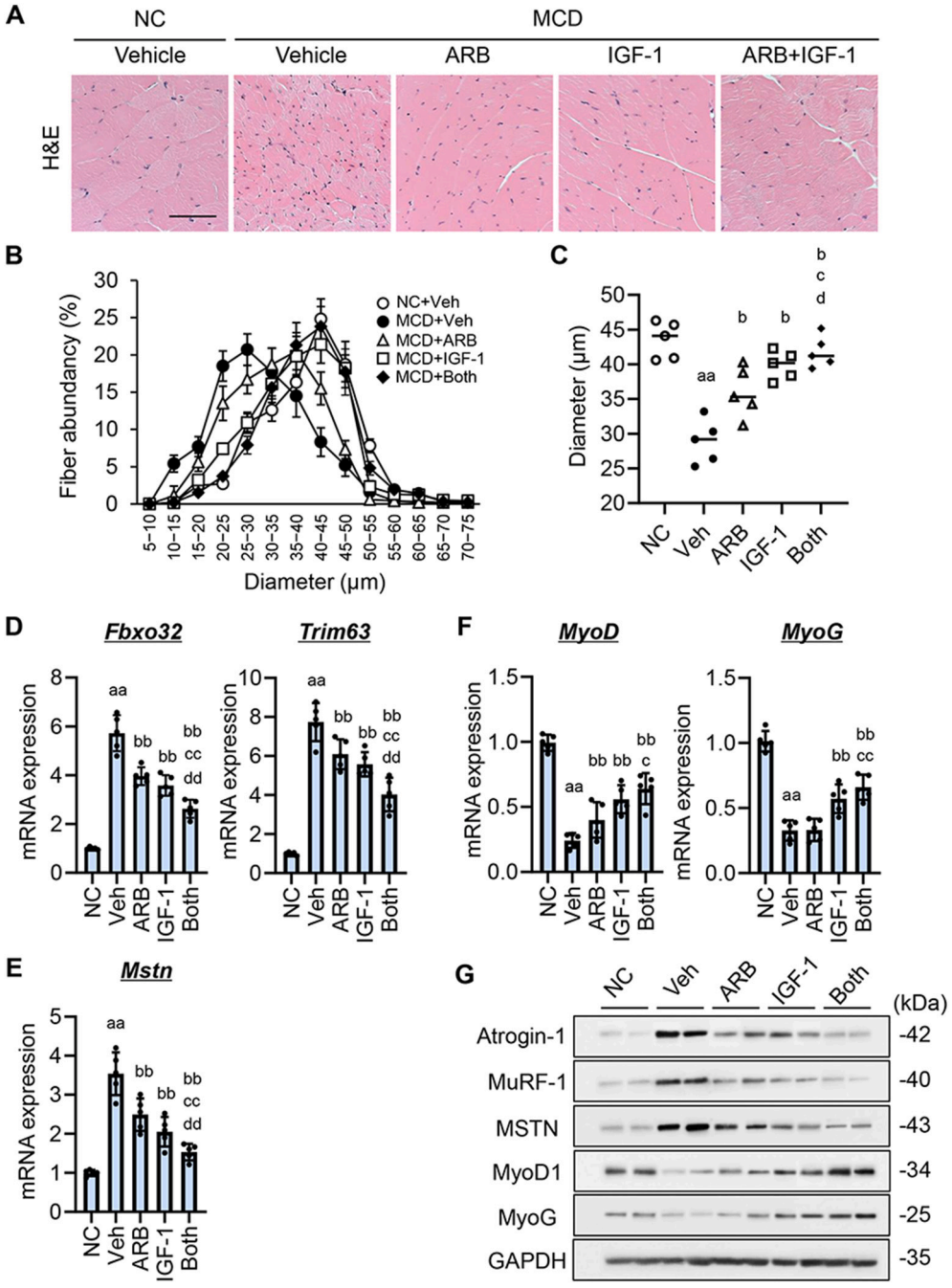

Fig. 3. Effect of ARB and IGF-1 on MCD-induced skeletal muscle fiber atrophy. (A) Representative micrographs of hematoxylin and eosin (H&E)-stained gastrocnemius muscle sections. Scale bar: 50 μm. (B) The minimum ferret diameter of the gastrocnemius muscle cross section was measured in the muscle transverse section. Fiber diameters were grouped from 0 to 75 μm, and values were expressed as a percentage of total fibers. (C) Average value of minimal Feret diameters of gastrocnemius muscle fiber. (D–F) Relative mRNA expression levels of (D) *Fbxo32* and *Trim63*, (E) *Mstn*, and (F) *MyoD* and *MyoG* in the gastrocnemius muscle of experimental mice. *Gapdh* was used as an internal control for qRT-PCR. (G) Western blots for Atrogin-1, MuRF-1, MSTN, MyoD1 and MyoG in gastrocnemius muscle tissues. GAPDH was used as the loading control for western blot analysis. Quantitative values are indicated as fold changes to the values of NC + Veh group (D–F). Data are the mean ± SD ($n = 5$). NC, normal chow; MCD, methionine-choline deficient diet; Veh, vehicle; ARB, angiotensin receptor blocker; IGF-1, insulin-like growth factor 1; Both, combination with ARB and IGF-1. aa; $p < 0.01$ vs NC, b; $p < 0.05$ vs Veh, bb; $p < 0.01$vs Veh, c; $p < 0.05$ vs ARB, cc; $p < 0.01$ vs ARB, d; $p < 0.05$ vs IGF-1, dd; $p < 0.01$ vs IGF-1 using Mann–Whitney *U* test.

MyoD1 and MyoG were decreased in the gastrocnemius muscle tissues of the MCD diet-fed mice; this was ameliorated by treatment with ARB and IGF-1 (Fig. 3F). These changes in gene expressions coincided with the intramuscular protein levels, indicating that treatment with ARB and IGF-1 effectively attenuated the increase in E3 ubiquitin ligases, and MSTN as well as the decrease in the myogenic factors in the MCD diet-fed mice (Fig. 3G).

3.4. ARB and IGF-1 interfere with FOXO transcription and augment AKT-mTOR signaling activation in the skeletal muscle of the MCD diet-fed mice

The E3 ubiquitin ligases had been recognized to be transcriptionally regulated by FOXO1 and FOXO3a [31], which are activated by translocating from the cytoplasm to the nuclei. Immunohistochemical analysis of the gastrocnemius fibers indicated that the localization of both

FOXO1 and FOXO3a was predominant in the cytoplasm but limited in the nuclei in the NC diet-fed mice, whereas these FOXOs were substantially localized in the nuclei in the MCD diet-fed mice (Fig. 4A–C). The substantial nuclear localization of the FOXOs in the MCD diet-fed mice suggested the transcriptional activation of FOXO1 and FOXO3a. Fig. 4D and E show increased transcriptional activities of FOXO1 and FOXO3 in the nuclear extract from the gastrocnemius muscle tissues of the MCD diet-fed mice. Notably, treatment with ARB and IGF-1 efficiently suppressed the intranuclear translocation and transcriptional activities of FOXO1 and FOXO3a in the gastrocnemius fibers of the MCD

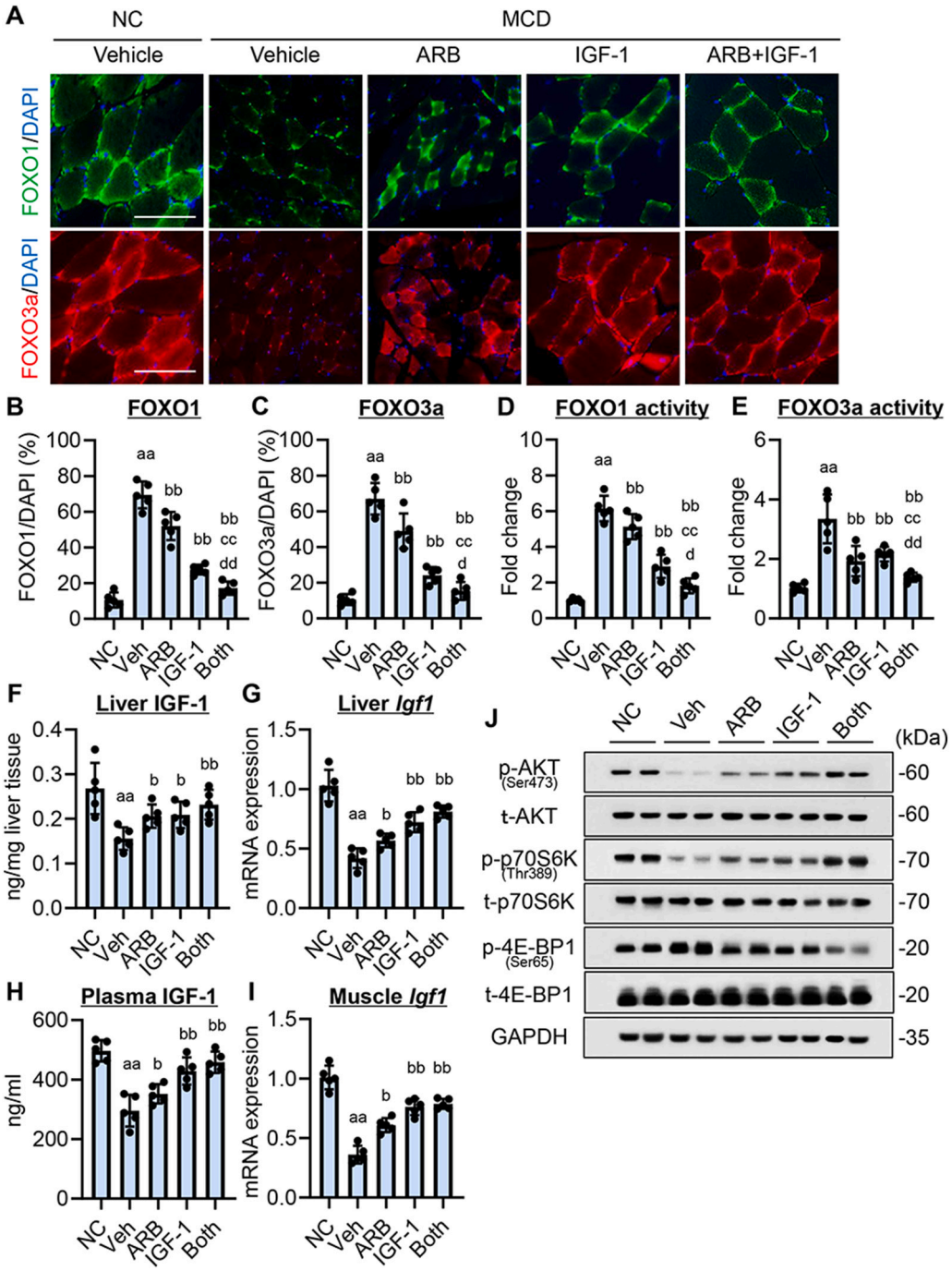

Fig. 4. Effect of ARB and IGF-1 on FOXOs transcriptional activity and IGF-1/AKT/mTOR signaling activation in gastrocnemius muscle. (A) Representative micrographs of immunofluorescent staining of FOXO1/DAPI (upper panel) and FOXO3a/DAPI (lower panel) in gastrocnemius muscle. Scale bar; 50 μm. (B, C) Semi-quantification of (B) FOXO1 and (C) FOXO3a positive nuclei in high magnification field of view. The ratio of FOXO1/DAPI or FOXO3a/DAPI positive myocytes per 50 DAPI positive myocytes in HPF was calculated. Five field sections per section were included in the quantitative analysis. (D, E) Measurement of transcriptional activities of (D) FOXO1 and (E) FOXO3 in the nuclear extract from the gastrocnemius muscle tissues. (F) Hepatic content of IGF-1. (G) Relative hepatic mRNA level of *Igf1*. (H) Plasma concentration of IGF-1. (I) Relative muscular mRNA level of *Igf1*. (J) Western blots for the phosphorylation of AKT, p70S6K, and 4E-BP1 in gastrocnemius muscle tissues. *Gapdh* was used as an internal control for qRT-PCR (G, I). GAPDH was used as the loading control for western blot analysis (J). Quantitative values are indicated as fold changes to the values of NC + Veh group (D, E, G, I). Data are the mean ± SD (n = 5). NC, normal chow; MCD, methionine-choline deficient diet; Veh, vehicle; ARB, angiotensin receptor blocker; IGF-1, insulin-like growth factor 1; Both, combination with ARB and IGF-1. aa; $p < 0.01$ vs NC, b; $p < 0.05$ vs Veh, bb; $p < 0.01$vs Veh, cc; $p < 0.01$ vs ARB, d; $p < 0.05$ vs IGF-1, dd; $p < 0.01$ vs IGF-1 using Mann–Whitney *U* test.

diet-fed mice (Fig. 4A–E).

Furthermore, we evaluated the effects of ARB and IGF-1 on the pathway of protein synthesis in gastrocnemius muscle tissues of the MCD diet-fed mice. IGF-1 facilitates skeletal muscle protein synthesis through the PI3K/AKT/mTOR pathway [11]. In the MCD diet-fed mice, the hepatic expression of *Igf1* and production of IGF-1 decreased along with the development of steatohepatitis; consequently, plasma IGF-1 level was lower in the MCD diet-fed mice than in the NC diet-fed mice (Fig. 4F–H). Interestingly, administration of human IGF-1 increased the plasma mouse IGF-1 level as well as augmented hepatic IGF-1 expression and production (Fig. 4F–H). Correspondingly to these increase in plasma and hepatic IGF-1, the expression of *Igf1* was increased in the gastrocnemius muscle tissues by treatment with IGF-1 (Fig. 4I). Likewise, treatment with ARB also increased the muscular *Igf1* expression according to hepatic and plasma IGF-1 levels in the MCD diet-fed mice (Fig. 4F–I). These findings suggest that treatment with ARB and IGF-1 boosted the upregulation of murine endogenous IGF-1 by improvement of hepatic function.

Along with the increase in IGF-1 levels, treatment with ARB and IGF-1 enhanced the phosphorylation of AKT in the gastrocnemius muscle tissues of the MCD diet-fed mice. Moreover, we found that treatment with ARB and IGF-1 promoted the phosphorylation of p70S6K^{Thr389} and repressed the phosphorylation of 4E-BP1^{Ser65}; these indicated the sequential activation of mTOR followed by IGF-1/ AKT signaling activation in the gastrocnemius muscle tissues of the MCD diet-fed mice (Fig. 4H).

3.5. ARB and IGF-1 inhibit the inflammatory and oxidative responses in the skeletal muscle of the MCD diet-fed mice

Hepatic injury-derived skeletal muscle atrophy is often associated with proinflammatory signaling [32]. Increased mRNA levels of TNFα, IL6, and IL1β were observed in the gastrocnemius muscle tissues of the MCD diet-fed mice; this was ameliorated by treatment with ARB and IGF-1 (Fig. 5A–C). An MCD diet is known to induce marked accumulation of ROS in mice [33]. Given that ARB and IGF-1 reduced hepatic ROS accumulation, we next evaluated the markers of antioxidant activity and chronic oxidative damage in the gastrocnemius muscle tissue. The mRNA levels of the antioxidant genes *Cat*, *Gpx1*, *Sod2*, and *Cytb* were significantly lower in the MCD diet-fed mice than in the NC diet-fed mice (Fig. 5D–G). Single treatment with ARB or IGF-1 increased the expressions of these antioxidant genes, and combined treatment more potently increased the expressions *Cat* and *Sod2* (Fig. 5D–G). Along with these effects on gene expression, the mean Trolox equivalent antioxidant capacity significantly increased after treatment with ARB and IGF-1 (Fig. 5H). Furthermore, the intramuscular levels of MDA in the gastrocnemius muscle were higher in the MCD diet-fed mice than in the NC diet-fed mice; this increase in the MDA level was ameliorated by treatment with ARB and IGF-1 (Fig. 5I). To uncover the mechanism of the antioxidant effect, we further analyzed dysfunction in the NADPH oxidases (NOXs), which is major sources of ROS in atrophied skeletal muscles. The intramuscular mRNA levels of *Nox2* and *Nox4* were higher in the MCD diet-fed mice than in the NC diet-fed mice, whereas the *Nox1* mRNA level was not altered (Fig. 5J–L). Treatment with ARB and IGF-1 significantly decreased *Nox2* expression but not *Nox4* expression in the gastrocnemius muscle of the MCD diet-fed mice (Fig. 5K and L).

3.6. ARB and IGF-1 improve mitochondrial dysfunction in the gastrocnemius muscle of the MCD diet-fed mice

Mitochondrial remodeling is crucial to meet the bioenergetic demand to support muscle homeostasis following injury [34]. The mtDNA copy number, an index of mitochondrial biogenesis, was remarkably decreased in the gastrocnemius muscle of the MCD diet-fed mice (Fig. 6A). This decrease in the mtDNA copy number was effectively ameliorated by treatment with ARB and IGF-1 (Fig. 6A). In addition, MCD diet feeding reduced the intramuscular protein levels of the mitochondrial biosynthesis-related markers, including PGC-1α, mtTFA, TFEB, and COX7A1; the levels of these proteins were restored by treatment with ARB and IGF-1 (Fig. 6B). Moreover, we found that treatment with ARB and IGF-1 increased the expressions of the genes that coded these mitochondrial biosynthesis-related markers (i.e., *Ppargc1a*, *Tfam*, *Tfb1m*, and *Cox7a1*) (Fig. 6C–F).

Furthermore, we examined the change in mitochondrial fission and fusion to evaluate the effect of both agents on mitochondrial dynamics. As shown in Fig. 6G, the intramuscular protein level of DRP1 was increased, while the level of MFN2 was decreased in the MCD diet-fed mice as compared to the NC diet-fed mice. These results suggested that MCD diet feeding disrupted the balance of mitochondrial dynamics by promoting the fission and preventing the fission. Notably, these MCD diet-induced mitochondrial fusion and fission imbalance was suppressed by treatment with ARB and IGF-1 (Fig. 6G). The suppression of mitochondrial dynamics imbalance by ARB and IGF-1 was also found at mRNA levels (Fig. 6H and I). Meanwhile, the muscular expression levels of LC31/LC3-II and PINK1 were not changed in MCD diet-fed mice and not modified by treatment with ARB and IGF-1, indicating that autophagy and mitophagy were limitedly involved in skeletal muscle homeostasis in the present model (Fig. 6G, J and K).

4. Discussion

Our study illustrated that combination of IGF-1 replacement with ARB potentiated myotrophic activity in an MCD diet-fed mice model of NASH-derived sarcopenia. An MCD diet is the classic dietary model that causes histological steatohepatitis and substantially mimics human NASH, which is characterized by reduced glycogen stores and peroxidant proteins, ROS accumulation, mitochondrial DNA dysfunction, and apoptosis [35]. Our findings showed that chronic feeding of an MCD diet induced a significant reduction in body weight and skeletal muscle mass. Several reports have claimed that dietary methionine restriction could improve skeletal muscle glucose metabolism in middle-aged mice [36,37]. On the other hand, choline deficiency has been shown to compromise cell membranes and impair growth and function in skeletal muscle [38]. Moreover, the lack of methionine and choline has been reported to induce the hepatic expression of ATII, which promotes skeletal muscle wasting [39]. Given these insights, MCD diet-induced skeletal muscle wasting can be attributed to mainly choline deficiency and hepatic dysfunction rather than methionine deficiency in this model.

Based on the results, we postulated that the antisarcopenic effect of ARB and IGF-1 was mediated by hepatoprotective and muscle-protective properties in the MCD diet-fed mice (Fig. 7). Our MCD diet-induced steatohepatitis model showed that both ARB and IGF-1 efficiently suppressed hepatic steatosis, hepatocyte apoptosis, and fibrosis development. A large number of studies showed an inhibitory effect of ARBs on the progression of steatohepatitis by suppressing ROS accumulation in both obese and nonobese NASH rodent models [26,40]. Moreover, a recent meta-analysis demonstrated that losartan could reduce the level of hepatic enzymes in patients with NAFLD [41]. Meanwhile, IGF-1 was reported to exert an inhibitory effect on NASH progression [15,23,42]. Consistent with these reports, we found that ARB and IGF-1 attenuated hepatic steatosis, hepatocyte apoptosis, and fibrosis, along with decreased ROS accumulation. The resulting increase in hepatic and plasma IGF-1 levels could contribute to the improvement of skeletal muscle wasting. Moreover, GDF15, a hepatokine increasing in NAFLD, has also suggested to play a key role in sarcopenia [43,44]. Notably, treatment with ARB and IGF-1 significantly reduced hepatic *Gdf15* expression reflecting the attenuation of mitochondrial stress by both agents in in MCD diet-fed mice. These findings also implicate the possible involvement of muscle-liver crosstalk in the anti-sarcopenic effect of ARB and IGF-1 replacement.

ARB and IGF-1 suppressed ubiquitin proteasome-mediated skeletal

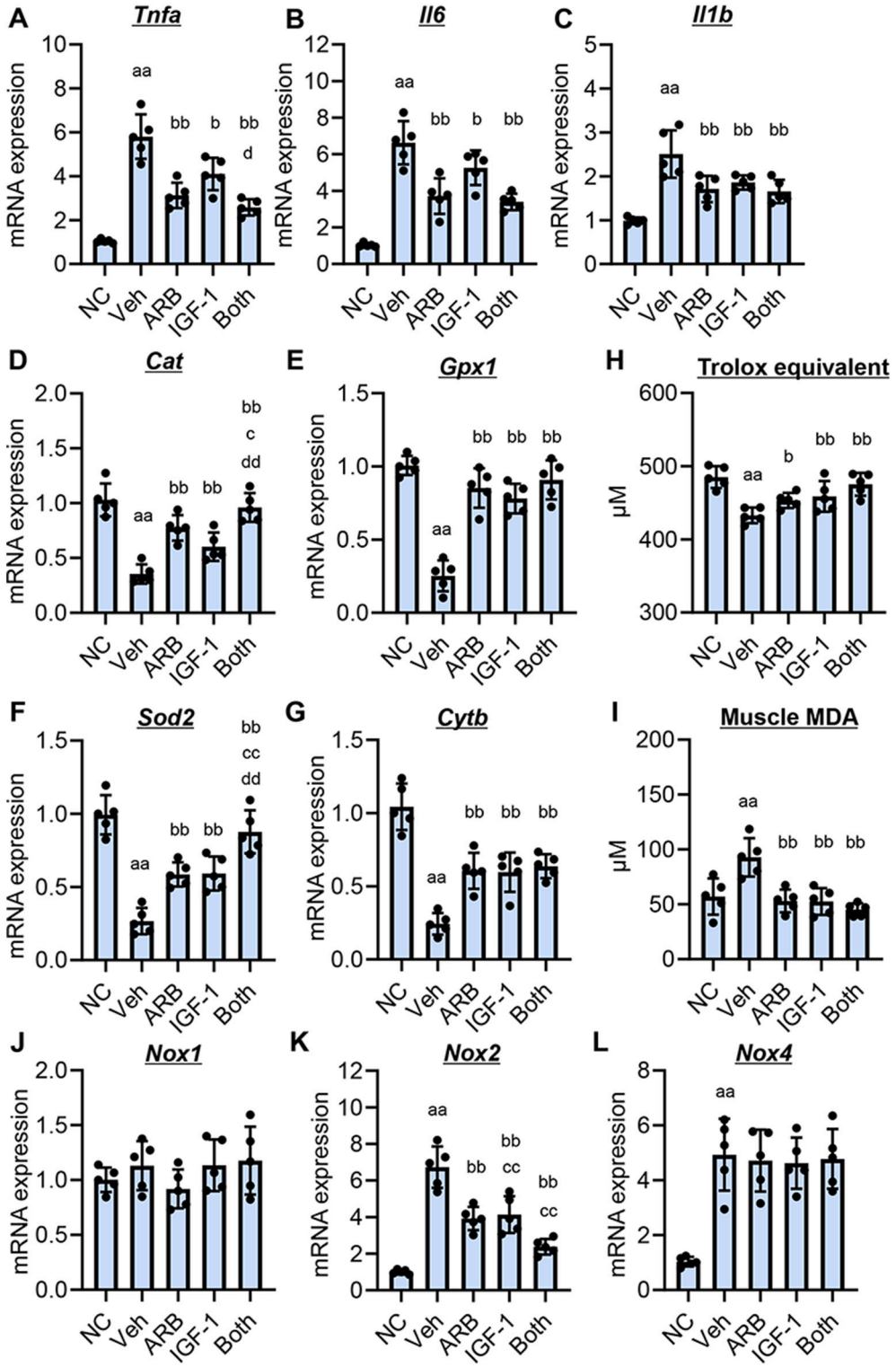

Fig. 5. Effect of ARB and IGF-1 on proinflammatory and oxidative responses in gastrocnemius muscle. (A–C) Relative mRNA expression levels of (A) *Tnfa*, (B) *Il6*, and (C) *Il1b* in the gastrocnemius muscle. (D–G) Relative mRNA expression levels of (D) *Cat*, (E) *Gpx1*, (F) *Sod2*, and (G) *Cytb* in the gastrocnemius muscle. (H) Trolox equivalent antioxidant capacity in the gastrocnemius muscle. (I) Malondialdehyde (MDA) contents in the gastrocnemius muscle. (J–L) Relative mRNA expression levels of (J) *Nox1*, (K) *Nox2*, and (L) *Nox4* in the gastrocnemius muscle. *Gapdh* was used as an internal control for qRT-PCR (A–G, J–L). Quantitative values are indicated as fold changes to the values of NC + Veh group (A–G, J–L). Data are the mean ± SD (n = 5). NC, normal chow; MCD, methionine-choline deficient diet; Veh, vehicle; ARB, angiotensin receptor blocker; IGF-1, insulin-like growth factor 1; Both, combination with ARB and IGF-1. aa; $p < 0.01$ vs NC, b; $p < 0.05$ vs Veh, bb; $p < 0.01$vs Veh, c; $p < 0.05$ vs ARB, cc; $p < 0.01$ vs ARB, d; $p < 0.05$ vs IGF-1, dd; $p < 0.01$ vs IGF-1 using Mann–Whitney *U* test.

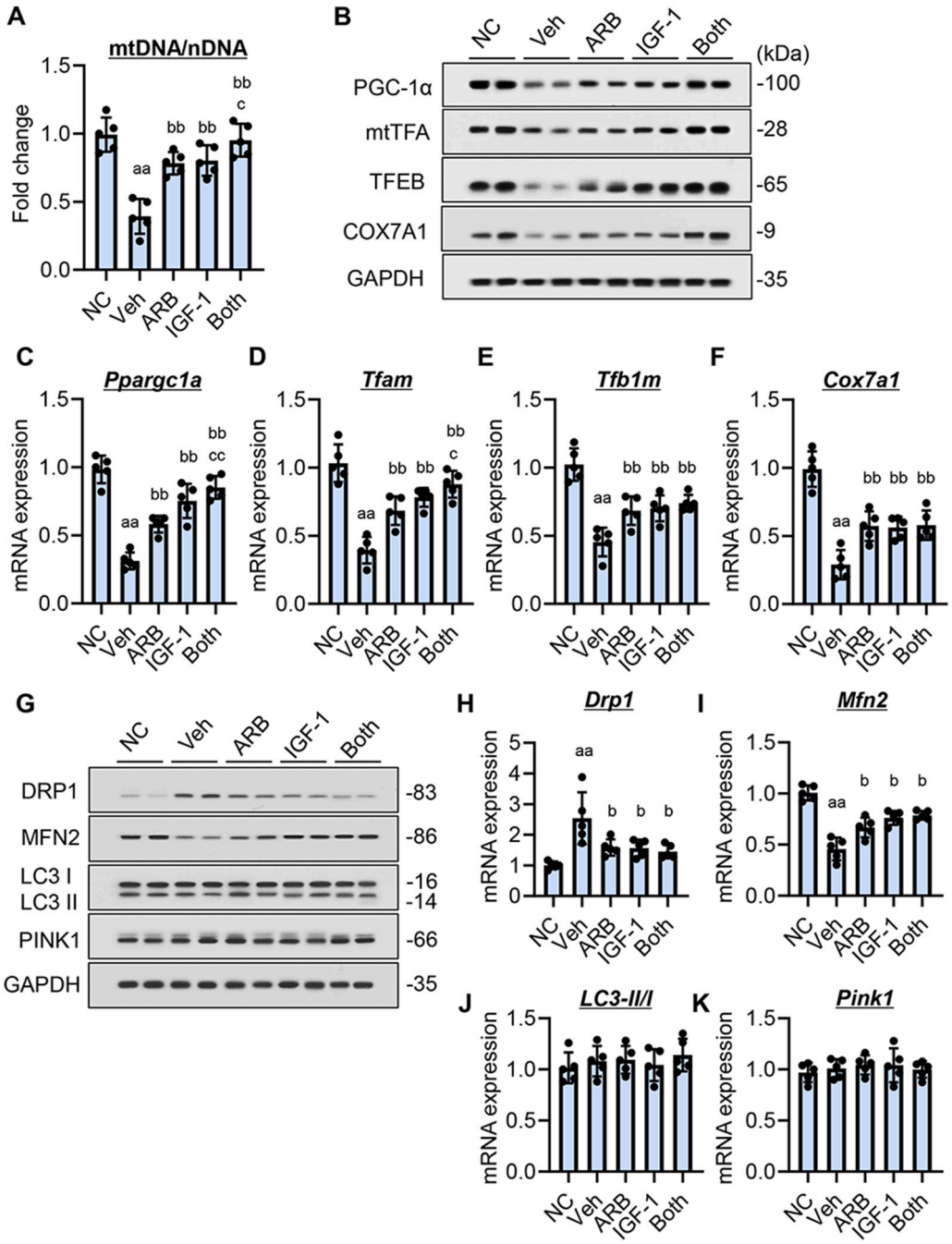

Fig. 6. Effect of ARB and IGF-1 on mitochondrial dysfunction in gastrocnemius muscle. (A) The mitochondrial DNA (mtDNA) copy number was assessed by RT-qPCR according to mtDNA (Cox2)/nuclear DNA (nDNA) (Ppia). (B) Western blots for PGC-1a, mtTFA, TFEB, and COX7A1 in gastrocnemius muscle. (C–F) Relative mRNA expression levels of (C) *Ppargc1a*, (D) *Tfam*, and (E) *Tfb1m*, and (F) *Cox7a1* in the gastrocnemius muscle. (G) Western blots for DRP1, MFN2, LC3-I/II, and PINK1 in gastrocnemius muscle. (H–K) Relative mRNA expression levels of (H) Drp1, (I) Mfn2, (J) ratio of LC3-II/I, and (K) Pink1 in the gastrocnemius muscle. *Gapdh* was used as an internal control for qRT-PCR (C–F, H–K). GAPDH was used as the loading control for western blot analysis (B, G). Quantitative values are indicated as fold changes to the values of NC + Veh group (C–F, H–K). Data are the mean ± SD (n = 5). NC, normal chow; MCD, methionine-choline deficient diet; Veh, vehicle; ARB, angiotensin receptor blocker; IGF-1, insulin-like growth factor 1; Both, combination with ARB and IGF-1. aa; $p < 0.01$ vs NC, b; $p < 0.05$ vs Veh, bb; $p < 0.01$vs Veh, c; $p < 0.05$ vs ARB, cc; $p < 0.01$ vs ARB, d; $p < 0.05$ vs IGF-1, dd; $p < 0.01$ vs IGF-1 using Mann–Whitney *U* test.

muscle atrophy by inhibiting the transcriptional activities of FOXO1 and FOXO3a. Both FOXOs are known to negatively regulate skeletal muscle mass and function by inducing the expression of the ubiquitin ligases atrogin-1 and MuRF-1 [11,20,26]. IGF-1/ AKT acts as a key signal to repress the activation of FOXOs by translocating to the cytoplasm [11,26,42]. Meanwhile, ATII induces skeletal muscle protein degradation, which is characterized by FOXO activation and upregulation of ubiquitin ligases [32]. Furthermore, previous reports suggested a mutual relationship between IGF-1/ AKT /mTOR activation and ATII blockade in the regulation of skeletal muscle homeostasis [32,45]. On the basis of these mechanistic interactions, we found that addition of ARB potently enhanced the inhibitory effect of IGF-1 replacement on FOXO-mediated upregulation of ubiquitin ligases and the IGF-1-mediated skeletal muscle protein synthesis through AKT/mTOR signaling activation. These findings indicated that combination with ARB potentiates both the anticatabolic and proanabolic effects of IGF-1

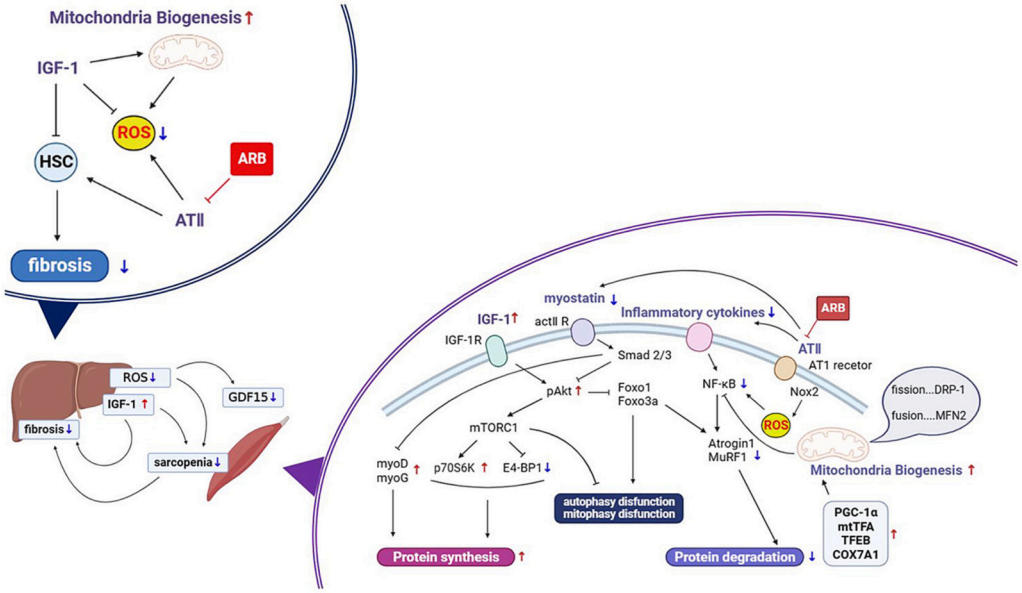

Fig. 7. Graphic representation of the effects of ARB and IGF-1 on NASH-derived skeletal muscle atrophy.

replacement on MCD diet-induced skeletal muscle atrophy.

We focused on inflammatory response and oxidative stress as the mechanisms underlying the effect of ARB and IGF-1 on skeletal muscle atrophy. Inflammatory cytokines, including TNFα, IL6, and IL1β, are released during NASH progression and hinder protein synthesis and degradation [32,46]. They activate various pathways, including the NF-κB, p38-MAPK, and MSTN pathways, to induce proteolysis through the ubiquitin proteasome system [32]. NASH-derived ROS accumulation is also associated with loss of skeletal muscle function [47]. Activation of the catabolic regulatory elements, such as FOXOs, NF-κB, and AMPK, by oxidative stress lead to muscle protein catabolism through the ubiquitin proteasome system [48,49]. In this study, ARB and IGF-1 effectively reduced the expressions of inflammatory cytokines, suppressed ROS accumulation, and restored the antioxidant capacity of the skeletal muscle in the MCD diet-fed mice. Furthermore, we investigated the effects of ARB and IGF-1 on NOXs and mitochondrial dysfunction, which are different sources of ROS [50,51]. The MCD diet-fed mice showed increased muscular expressions of *Nox2* and *Nox4*, whereas treatment with ARB and IGF-1 reduced the expression of *Nox2* but not *Nox4*. NOX2 is the main source of ROS during muscle fiber atrophy and contractile dysfunction in a disease state, whereas NOX4 is required for overload-induced skeletal muscle hypertrophy [50]. Therefore, downregulation of NOX2 considerably contributed to the suppression of ROS accumulation in this model.

Mitochondrial biogenesis is indispensable for regular muscle function, and mitochondrial dysfunction brings about muscle atrophy through the activation of various catabolic pathways [51]. Mitochondrial biogenesis is mainly regulated by PGC-1α, which activates nuclear respiratory factors and estrogen-related receptor-α, which further activates TFAM to promote mtDNA replication [52]. We and another group have shown the ATII-induced reduction of mitochondria content which is suppressed by ARB [26,53]. A recent study has also reported that IGF-1 signaling activation facilitated mitochondrial biogenesis and increased mitochondria content through upregulation of PGC-1α, leading to increased myogenic differentiation efficacy [54]. In accordance with these evidences, combination of ARB and IGF-1 inhibited the MCD diet-induced reduction of mitochondria content indicated with mtDNA/nDNA along with increased expressions of mitochondrial biogenesis-related markers in skeletal muscle. Moreover, we found that the MCD diet consuming conferred the imbalance of mitochondrial dynamics; the increasing mitochondrial fission and decreasing fusion in skeletal muscle in consistent with the results of recent report [55]. It was noteworthy that treatment with ARB and IGF-1 efficiently inhibited the MCD diet-induced imbalance of mitochondrial dynamics. These findings indicate that normalization of mitochondrial biogenesis and dynamics is involved in the antisarcopenic effect of ARB and IGF-1 replacement.

It should be noted that there are several limitations to our study. First, with respect to the antisarcopenic effect of ARB, it is still unclear which is more predominant, the effect via improvement of liver pathology or the direct effect on skeletal muscle. Actually, the gene expression levels of ATII receptor were higher in the liver than in the skeletal muscle in the MCD diet-fed mice (data not shown). This result leads to speculate that treatment of ARB possibly has a greater effect against NASH-related liver injury than direct action to skeletal muscle. Second, the carcinogenic risk of clinical application of this combination regimen may be of concern. Although IGF-1 administration was not observed to promote hepatic carcinogenesis in the MCD diet-fed mice, activation of the IGF-1 signaling cascade has been suggested to promote the growth and metastasis of hepatocellular carcinoma through upregulation of downstream mitogens, including MAPK and PI3K/ AKT [56].

5. Conclusions

Pharmacological blockade of ATII by ARB augmented the inhibitory effect of IGF-1 replacement in NASH-derived sarcopenia. This effect was based on multiple functional properties, including upregulation of IGF-1 and reduction of ROS, which are derived from the hepatoprotective effect; inhibition of FOXO activation, inflammatory response, and oxidative stress; and promotion of mitochondrial biogenesis. This combination regimen could be a therapeutic approach for preventing skeletal muscle atrophy in NASH-derived sarcopenia.

Funding

This study was partially supported by a Grant-in-Aid for Research on Hepatitis from the Japan Agency for Medical Research and Development (JP23fk0210128s0201).

CRediT authorship contribution statement

Misako Tanaka: Data curation, Formal analysis, Investigation, Methodology, Writing – original draft. **Kosuke Kaji:** Conceptualization,

Data curation, Methodology, Supervision, Validation, Visualization, Writing – review & editing. **Norihisa Nishimura:** Formal analysis, Investigation, Writing – review & editing. **Shohei Asada:** Investigation, Writing – review & editing. **Aritoshi Koizumi:** Investigation, Writing – review & editing. **Takuya Matsuda:** Investigation, Writing – review & editing. **Nobuyuki Yorioka:** Investigation, Writing – review & editing. **Yuki Tsuji:** Software, Writing – review & editing. **Yukihisa Fujinaga:** Formal analysis, Visualization, Writing – review & editing. **Shinya Sato:** Resources, Validation, Writing – review & editing. **Tadashi Namisaki:** Methodology, Writing – review & editing. **Takemi Akahane:** Supervision, Writing – review & editing. **Hitoshi Yoshiji:** Conceptualization, Supervision, Writing – review & editing.

Declaration of competing interest

No potential conflicts of interest were disclosed by all authors.

Data availability

Data will be made available on request.

Acknowledgements

The authors would like to thank Enago (www.enago.jp) for the English language review.

Appendix A. Supplementary data

Supplementary data to this article can be found online at https://doi.org/10.1016/j.bbamcr.2023.119649.

References

[1] V.T. Samuel, G.I. Shulman, Nonalcoholic fatty liver disease, insulin resistance, and ceramides, N. Engl. J. Med. 381 (2019) 1866–1869.
[2] S. Raza, S. Rajak, A. Upadhyay, A. Tewari, R.A. Sinha. Current treatment paradigms and emerging therapies for NAFLD/NASH, Front. Biosci. (Landmark edition), 26 (2021) 206–237.
[3] S. Yamamura, T. Kawaguchi, D. Nakano, Y. Tomiyasu, S. Yoshinaga, Y. Doi, H. Takahashi, K. Anzai, Y. Eguchi, T. Torimura, N. Shiba, Profiles of advanced hepatic fibrosis evaluated by FIB-4 index and shear wave elastography in health checkup examinees, Hepatol. Res. 50 (2020) 199–213.
[4] A.J. Cruz-Jentoft, J.P. Baeyens, J.M. Bauer, Y. Boirie, T. Cederholm, F. Landi, F. C. Martin, J.P. Michel, Y. Rolland, S.M. Schneider, E. Topinková, M. Vandewoude, M. Zamboni, Sarcopenia: European consensus on definition and diagnosis: report of the European working group on sarcopenia in older people, Age Ageing 39 (2010) 412–423.
[5] B.K. Koo, D. Kim, S.K. Joo, J.H. Kim, M.S. Chang, B.G. Kim, K.L. Lee, W. Kim, Sarcopenia is an independent risk factor for non-alcoholic steatohepatitis and significant fibrosis, J. Hepatol. 66 (2017) 123–131.
[6] S. Petta, S. Ciminnisi, V. Di Marco, D. Cabibi, C. Cammà, A. Licata, G. Marchesini, A. Craxì, Sarcopenia is associated with severe liver fibrosis in patients with non-alcoholic fatty liver disease, Aliment. Pharmacol. Ther. 45 (2017) 510–518.
[7] Y.H. Lee, S.U. Kim, K. Song, J.Y. Park, D.Y. Kim, S.H. Ahn, B.W. Lee, E.S. Kang, B. S. Cha, K.H. Han, Sarcopenia is associated with significant liver fibrosis independently of obesity and insulin resistance in nonalcoholic fatty liver disease: Nationwide surveys (KNHANES 2008-2011), Hepatology (Baltimore, Md.) 63 (2016) 776–786.
[8] S.L. Allen, J.I. Quinlan, A. Dhaliwal, M.J. Armstrong, A.M. Elsharkawy, C.A. Greig, J.M. Lord, G.G. Lavery, L. Breen, Sarcopenia in chronic liver disease: mechanisms and countermeasures, American journal of physiology, Am. J. Physiol. Gastrointest. Liver Physiol. 320 (2021) G241–g257.
[9] Y. Kitajima, H. Takahashi, T. Akiyama, K. Murayama, S. Iwane, T. Kuwashiro, K. Tanaka, S. Kawazoe, N. Ono, T. Eguchi, K. Anzai, Y. Eguchi, Supplementation with branched-chain amino acids ameliorates hypoalbuminemia, prevents sarcopenia, and reduces fat accumulation in the skeletal muscles of patients with liver cirrhosis, J. Gastroenterol. 53 (2018) 427–437.
[10] Y. Nishida, Y. Ide, M. Okada, T. Otsuka, Y. Eguchi, I. Ozaki, K. Tanaka, T. Mizuta, Effects of home-based exercise and branched-chain amino acid supplementation on aerobic capacity and glycemic control in patients with cirrhosis, Hepatol. Res. 47 (2017) E193–E200.
[11] T. Yoshida, P. Delafontaine, Mechanisms of IGF-1-mediated regulation of skeletal muscle hypertrophy and atrophy, Cells 9 (2020).
[12] C.Y. Ewald, J.N. Landis, J. Porter Abate, C.T. Murphy, T.K. Blackwell, Dauer-independent insulin/IGF-1-signalling implicates collagen remodelling in longevity, Nature 519 (2015) 97–101.
[13] A. Adamek, A. Kasprzak, Insulin-like growth factor (IGF) system in liver diseases, Int. J. Mol. Sci. 19 (2018).
[14] M.L. Hribal, T. Procopio, S. Petta, A. Sciacqua, S. Grimaudo, R.M. Pipitone, F. Perticone, G. Sesti, Insulin-like growth factor-I, inflammatory proteins, and fibrosis in subjects with nonalcoholic fatty liver disease, J. Clin. Endocrinol. Metab. 98 (2013) E304–E308.
[15] D. Cabrera, A. Ruiz, C. Cabello-Verrugio, E. Brandan, L. Estrada, M. Pizarro, N. Solis, J. Torres, F. Barrera, M. Arrese, Diet-induced nonalcoholic fatty liver disease is associated with sarcopenia and decreased serum insulin-like growth factor-1, Dig. Dis. Sci. 61 (2016) 3190–3198.
[16] C.D. McMahon, C. R, H.G. Radley-Crabb, W. T, K.G. Matthews, P.W. Sheard, S. Z, M. D, S.T. Grounds, Lifelong exercise and locally produced insulin-like growth factor-1 (IGF-1) have a modest influence on reducing age-related muscle wasting in mice, Scand. J. Med. Sci. Sports 24 (2014) e423–e435.
[17] E.S.A.C. Simões, A.S. Miranda, N.P. Rocha, A.L. Teixeira, Renin angiotensin system in liver diseases: friend or foe? World J. Gastroenterol. 23 (2017) 3396–3406.
[18] T. Kadoguchi, S. Kinugawa, S. Takada, A. Fukushima, T. Furihata, T. Homma, Y. Masaki, W. Mizushima, M. Nishikawa, M. Takahashi, T. Yokota, S. Matsushima, K. Okita, H. Tsutsui, Angiotensin II can directly induce mitochondrial dysfunction, decrease oxidative fibre number and induce atrophy in mouse hindlimb skeletal muscle, Exp. Physiol. 100 (2015) 312–322.
[19] O.K. Hwang, J.K. Park, E.J. Lee, E.M. Lee, A.Y. Kim, K.S. Jeong, Therapeutic effect of losartan, an angiotensin II type 1 receptor antagonist, on CCl_4-induced skeletal muscle injury, Int. J. Mol. Sci. 17 (2016) 227.
[20] Y.H. Song, Y. Li, J. Du, W.E. Mitch, N. Rosenthal, P. Delafontaine, Muscle-specific expression of IGF-1 blocks angiotensin II-induced skeletal muscle wasting, J. Clin. Invest. 115 (2005) 451–458.
[21] Y.L. Lin, S.Y. Chen, Y.H. Lai, C.H. Wang, C.H. Kuo, H.H. Liou, B.G. Hsu, Angiotensin II receptor blockade is associated with preserved muscle strength in chronic hemodialysis patients, BMC Nephrol. 20 (2019) 54.
[22] M. Kitade, K. Kaji, N. Nishimura, K. Seki, K. Nakanishi, Y. Tsuji, S. Sato, S. Saikawa, H. Takaya, H. Kawaratani, T. Namisaki, K. Moriya, A. Mitoro, H. Yoshiji, Blocking development of liver fibrosis augments hepatic progenitor cell-derived liver regeneration in a mouse chronic liver injury model, Hepatol. Res. 49 (2019) 1034–1045.
[23] H. Nishizawa, G. Iguchi, H. Fukuoka, M. Takahashi, K. Suda, H. Bando, R. Matsumoto, K. Yoshida, Y. Odake, W. Ogawa, Y. Takahashi, IGF-I induces senescence of hepatic stellate cells and limits fibrosis in a p53-dependent manner, Sci. Rep. 6 (2016), 34605.
[24] S. Iwai, K. Kaji, N. Nishimura, T. Kubo, F. Tomooka, A. Shibamoto, J. Suzuki, Y. Tsuji, Y. Fujinaga, K. Kitagawa, T. Namisaki, T. Akahane, H. Yoshiji, Glucagon-like peptide-1 receptor agonist, semaglutide attenuates chronic liver disease-induced skeletal muscle atrophy in diabetic mice, Biochim. Biophys. Acta (BBA) - Mol. Basis Dis. 1869 (2023), 166770.
[25] B.A. Irving, J.Y. Weltman, D.W. Brock, C.K. Davis, G.A. Gaesser, A. Weltman, NIH ImageJ and Slice-O-Matic computed tomography imaging software to quantify soft tissue, Obesity (Silver Spring, Md.) 15 (2007) 370–376.
[26] S. Takeda, K. Kaji, N. Nishimura, M. Enomoto, Y. Fujimoto, K. Murata, H. Takaya, H. Kawaratani, K. Moriya, T. Namisaki, T. Akahane, H. Yoshiji, Angiotensin receptor blockers potentiate the protective effect of branched-chain amino acids on skeletal muscle atrophy in cirrhotic rats, Mol. Nutr. Food Res. 65 (2021), e2100526.
[27] E.M. Brunt, D.E. Kleiner, L.A. Wilson, P. Belt, B.A. Neuschwander-Tetri, Nonalcoholic fatty liver disease (NAFLD) activity score and the histopathologic diagnosis in NAFLD: distinct clinicopathologic meanings, Hepatology (Baltimore, Md.) 53 (2011) 810–820.
[28] T. Shimamura, Y. Sumikura, T. Yamazaki, A. Tada, T. Kashiwagi, H. Ishikawa, T. Matsui, N. Sugimoto, H. Akiyama, H. Ukeda, Applicability of the DPPH assay for evaluating the antioxidant capacity of food additives—inter-laboratory evaluation study, Anal. Sci. 30 (2014) 717–721.
[29] S.Y. Shi, S.Y. Lu, T. Sivasubramaniyam, X.S. Revelo, E.P. Cai, C.T. Luk, S. A. Schroer, P. Patel, R.H. Kim, E. Bombardier, J. Quadrilatero, A.R. Tupling, T. W. Mak, D.A. Winer, M. Woo, DJ-1 links muscle ROS production with metabolic reprogramming and systemic energy homeostasis in mice, Nat. Commun. 6 (2015) 7415.
[30] B.K. Koo, S.H. Um, D.S. Seo, S.K. Joo, J.M. Bae, J.H. Park, M.S. Chang, J.H. Kim, J. Lee, W.I. Jeong, W. Kim, Growth differentiation factor 15 predicts advanced fibrosis in biopsy-proven non-alcoholic fatty liver disease, Liver Int. 38 (2018) 695–705.
[31] J.P. Gumucio, C.L. Mendias, Atrogin-1, MuRF-1, and sarcopenia, Endocrine 43 (2013) 12–21.
[32] T. Yoshida, A.M. Tabony, S. Galvez, W.E. Mitch, Y. Higashi, S. Sukhanov, P. Delafontaine, Molecular mechanisms and signaling pathways of angiotensin II-induced muscle wasting: potential therapeutic targets for cardiac cachexia, Int. J. Biochem. Cell Biol. 45 (2013) 2322–2332.
[33] M. Inoue, S. Tazuma, K. Kanno, H. Hyogo, K. Igarashi, K. Chayama, Bach1 gene ablation reduces steatohepatitis in mouse MCD diet model, J. Clin. Biochem. Nutr. 48 (2011) 161–166.
[34] V. Romanello, M. Sandri, The connection between the dynamic remodeling of the mitochondrial network and the regulation of muscle mass, Cell. Mol. Life Sci. 78 (2021) 1305–1328.
[35] M.V. Machado, G.A. Michelotti, G. Xie, T. Almeida Pereira, J. Boursier, B. Bohnic, C.D. Guy, A.M. Diehl, Mouse models of diet-induced nonalcoholic steatohepatitis reproduce the heterogeneity of the human disease, PLoS One 10 (2015), e0127991.

[36] T. Luo, Y. Yang, Y. Xu, Q. Gao, G. Wu, Y. Jiang, J. Sun, Y. Shi, G. Le, Dietary methionine restriction improves glucose metabolism in the skeletal muscle of obese mice, Food Funct. 10 (2019) 2676–2690.
[37] A. Swaminathan, A. Fokin, T. Venckūnas, H. Degens, Methionine restriction plus overload improves skeletal muscle and metabolic health in old mice on a high fat diet, Sci. Rep. 11 (2021) 1260.
[38] A. Moretti, M. Paoletta, S. Liguori, M. Bertone, G. Toro, G. Iolascon, Choline: an essential nutrient for skeletal muscle, Nutrients 12 (2020).
[39] K.C. Lee, C.C. Chan, Y.Y. Yang, Y.C. Hsieh, Y.H. Huang, H.C. Lin, Aliskiren attenuates steatohepatitis and increases turnover of hepatic fat in mice fed with a methionine and choline deficient diet, PLoS One 8 (2013), e77817.
[40] J. Kato, M. Koda, M. Kishina, S. Tokunaga, T. Matono, T. Sugihara, M. Ueki, Y. Murawaki, Therapeutic effects of angiotensin II type 1 receptor blocker, irbesartan, on non-alcoholic steatohepatitis using FLS-Ob/Ob male mice, Int. J. Mol. Med. 30 (2012) 107–113.
[41] M.T. Dawn, J.J. Frances, C.S. Janet, D.W. Christopher, A.W. John, A.H. Stephen, Rosiglitazone versus rosiglitazone and metformin versus rosiglitazone and losartan in the treatment of nonalcoholic steatohepatitis in humans: a 12-month randomized, prospective, open-label trial, Hepatology (Baltimore, Md.) 54 (2011) 1631–1639.
[42] X. Luo, X. Jiang, J. Li, Y. Bai, Z. Li, P. Wei, S. Sun, Y. Liang, S. Han, X. Li, B. Zhang, Insulin-like growth factor-1 attenuates oxidative stress-induced hepatocyte premature senescence in liver fibrogenesis via regulating nuclear p53-progerin interaction, Cell Death Dis. 10 (2019) 451.
[43] S.H. Lee, J.Y. Lee, K.H. Lim, Y.S. Lee, J.M. Koh, Associations between plasma growth and differentiation Factor-15 with aging phenotypes in muscle, adipose tissue, and bone, Calcif. Tissue Int. 110 (2022) 236–243.
[44] M. Ost, C. Igual Gil, V. Coleman, S. Keipert, S. Efstathiou, V. Vidic, M. Weyers, S. Klaus, Muscle-derived GDF15 drives diurnal anorexia and systemic metabolic remodeling during mitochondrial stress, EMBO Rep. 21 (2020), e48804.
[45] T.N. Burks, E. Andres-Mateos, R. Marx, R. Mejias, C. Van Erp, J.L. Simmers, J. D. Walston, C.W. Ward, R.D. Cohn, Losartan restores skeletal muscle remodeling and protects against disuse atrophy in sarcopenia, Sci. Transl. Med. 3 (2011) 82ra37.
[46] S.H. Shen, T.Y. Zhong, C. Peng, J. Fang, B. Lv, Structural modulation of gut microbiota during alleviation of non-alcoholic fatty liver disease with Gynostemma pentaphyllum in rats, BMC Complement. Med. Ther. 20 (2020) 34.
[47] H. Nishikawa, H. Enomoto, S. Nishiguchi, H. Iijima, Sarcopenic obesity in liver cirrhosis: possible mechanism and clinical impact, Int. J. Mol. Sci. 22 (2021).
[48] J.M. McClung, A.R. Judge, S.K. Powers, Z. Yan, p38 MAPK links oxidative stress to autophagy-related gene expression in cachectic muscle wasting, Am. J. Phys. Cell Phys. 298 (2010) C542–C549.
[49] M. Zungu, J.C. Schisler, M.F. Essop, C. McCudden, C. Patterson, M.S. Willis, Regulation of AMPK by the ubiquitin proteasome system, Am. J. Pathol. 178 (2011) 4–11.
[50] L.F. Ferreira, O. Laitano, Regulation of NADPH oxidases in skeletal muscle, Free Radic. Biol. Med. 98 (2016) 18–28.
[51] E. Marzetti, R. Calvani, M. Cesari, T.W. Buford, M. Lorenzi, B.J. Behnke, C. Leeuwenburgh, Mitochondrial dysfunction and sarcopenia of aging: from signaling pathways to clinical trials, Int. J. Biochem. Cell Biol. 45 (2013) 2288–2301.
[52] L.D. Popov, Mitochondrial biogenesis: an update, J. Cell. Mol. Med. 24 (2020) 4892–4899.
[53] M. Mitsuishi, K. Miyashita, A. Muraki, H. Itoh, Angiotensin II reduces mitochondrial content in skeletal muscle and affects glycemic control, Diabetes 58 (2009) 710–717.
[54] X. Guan, Q. Yan, D. Wang, G. Du, J. Zhou, IGF-1 signaling regulates mitochondrial remodeling during myogenic differentiation, Nutrients 14 (2022).
[55] P. Zheng, W. Ma, Y. Gu, H. Wu, Z. Bian, N. Liu, D. Yang, X. Chen, High-fat diet causes mitochondrial damage and downregulation of mitofusin-2 and optic atrophy-1 in multiple organs, J. Clin. Biochem. Nutr. 73 (2023) 61–76.
[56] J. Wu, A.X. Zhu, Targeting insulin-like growth factor axis in hepatocellular carcinoma, J. Hematol. Oncol. 4 (2011) 30.